Materials Science and Engineering A 529 (2011) 81–87

Contents lists available at SciVerse ScienceDirect

Materials Science and Engineering A

journal homepage: www.elsevier.com/locate/msea

Resistance spot weld fatigue behavior and dislocation substructures in two different heats of AZ31 magnesium alloy

L. Xiao [a], L. Liu [a], D.L. Chen [b], S. Esmaeili [a], Y. Zhou [a,*]

[a] Department of Mechanical & Mechatronics Engineering, University of Waterloo, Waterloo, ON N2L 3G1, Canada
[b] Department of Mechanical and Industrial Engineering, Ryerson University, Toronto, ON M5B 2K3, Canada

ARTICLE INFO

Article history:
Received 1 May 2011
Received in revised form 29 August 2011
Accepted 30 August 2011
Available online 8 September 2011

Keywords:
Magnesium alloy
Resistance spot welding
Fatigue property
Dislocation structure
Microstructure

ABSTRACT

Fatigue life and dislocation substructure were evaluated in two groups of AZ31 Mg alloy resistance spot welds (heats SA and SB respectively, which had similar chemical compositions but different fusion zone microstructures). The results showed that the SA welds with a refined microstructure displayed a higher fatigue resistance than the SB welds when tested under conditions of higher cyclic load range causing interfacial failure across the fusion zone. TEM examinations revealed that typical dislocation configurations in the coarse-grained SB welds were parallel dislocation lines and parallelogram dislocation cells produced by basal slip, while elongated dislocation cells arising from basal and pyramidal multiple slips occurred in the SA welds. Twinning was observed to occur in both SA and SB welds, with more twins present in the SB welds. The strong slip incompatibilities between adjacent dendritic grains led to high local stress concentrations that activated twinning in the coarse-grained SB welds, while pyramidal slip together with twinning occurred in the fine-grained SA welds. This resulted in increased number and dispersion of slip systems which improved fatigue life in the SA welds.

1. Introduction

Magnesium (Mg) alloys, with an attractive high strength-to-weight ratio, are being increasingly used in automotive, aerospace, and electronics industries. Resistance spot welding is widely used in the automotive industry for producing thin sheet metal components and structures due to its advantages in welding productivity and robotization. However, the weldability of Mg alloy joined by conventional fusion welding is inferior to steel and aluminum alloys, because the well-developed columnar grains near the fusion boundary and coarse equiaxed dendritic grains formed in the fusion zone can seriously compromise the mechanical properties of joints in Mg alloys [1–4]. Fine grains are generally desirable to improve mechanical properties of welds [3–5]. Therefore, the microstructural refinement of Mg alloy welds has attracted a lot of attention in recent years [3–6].

In our previous work [3,4], it was observed that coarse Al_8Mn_5 particles promoted microstructure refinement and mechanical property improvement in comparing weldability of two AZ31 Mg alloys—SA and SB (SA from Supplier A and SB from Supplier B), which have a similar chemical composition but different scales of second-phase particles. The preexisting micro-sized Al_8Mn_5 intermetallic particles were observed to act as nucleation sites for α-Mg grain formation resulting in an early columnar-equiaxed-transition (CET) and refinement of microstructure in the fusion zone during solidification of the AZ31 Mg alloy welds [3]. However, it was unknown how and to what extent the refined microstructure affects fatigue properties. The structural application of welded Mg alloy joints requires a detailed understanding of the cyclic deformation resistance so as to predict fatigue life of welded structures, and to ensure the integrity and safety of welded structures in the automotive industry.

Both slip and twinning play an important role in maintaining homogeneous plastic deformation in hexagonal-close-packed (hcp) alloys [7]. It has been revealed that (0 0 0 2) basal slip is usually the dominant plastic deformation mode in cold deformed Mg alloys [8–13]. A recent study involving a fine-grained AZ31B Mg alloy has indicated that besides (0 0 0 2) basal slip, nonbasal glide could be activated to maintain the continuity of strain due to stress concentrations at the boundaries [8]. On the other hand, $\{1\,0\,\bar{1}\,2\}$ twinning was observed to be easily activated in a coarse-grained cast AZ91 Mg alloy under cyclic loading [9–11]. Twinning was more difficult with a smaller amount of twinning in a fine-grained material than in a coarse-grained one [9,12,13]. The objective of this study is to

* Corresponding author. Tel.: +1 519 8884567x36095; fax: +1 519 8855862.
E-mail address: nzhou@uwaterloo.ca (Y. Zhou).

0921-5093/$ – see front matter © 2011 Elsevier B.V. All rights reserved.
doi:10.1016/j.msea.2011.08.064

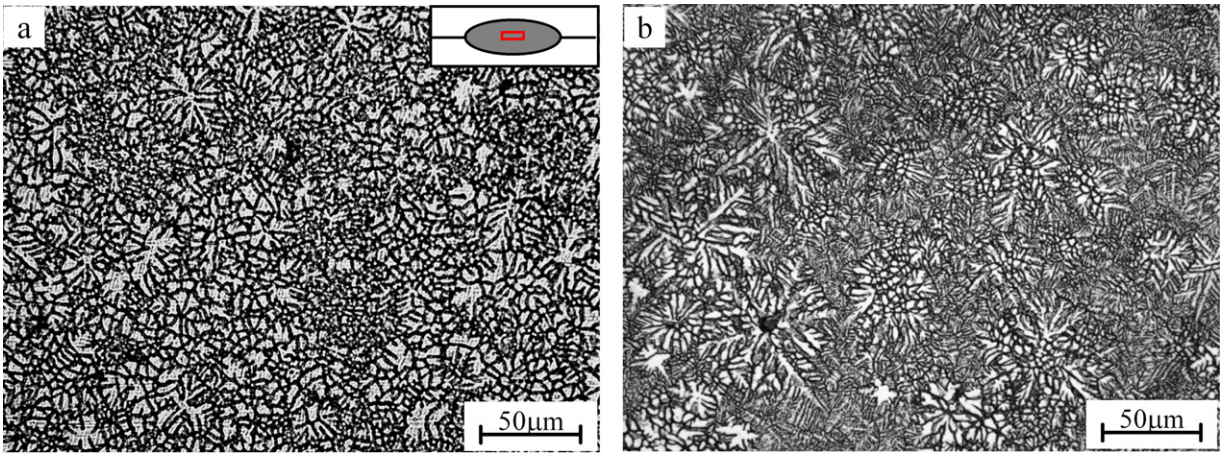

Fig. 1. Equiaxed dendritic structure in the fusion zone of AZ31 Mg alloy resistance spot welds: (a) SA with a thickness of 2 mm and (b) SB with a thickness of 1.5 mm. The location of the metallographs within the weld nuggets is indicated by a small rectangle inserted in the upper-right illustration.

examine the fatigue life of AZ31 Mg alloy resistance spot welds as well as the influence of microstructural refinement on slip and twinning deformation modes.

2. Experimental procedure

The materials used in this study were two commercial grade hot-rolled sheets of AZ31 Mg alloy in H24 temper with thicknesses of 2.0 mm (SA) and 1.5 mm (SB) respectively, which had similar optical microstructures and chemical compositions but different size scales of second-phase particles in the as-received material [3]. SA had coarser Al_8Mn_5 particles of 4–10 μm in length than SB [3]. The difference in particle size scales resulted in microstructural difference in the welds of the two alloys [3]. The diameter of equiaxed dendrites in the center of the fusion zones in SA welds was finer than that of SB, and the length of columnar dendrites in the vicinity of the fusion boundary in SA welds was also shorter than those of SB welds, as shown in Figs. 1(a) and (b), and 2(a) and (b). The average diameter of the flower-like dendrites was about 55 μm in alloy SA (Fig. 1(a)), and 85 μm in the SB alloy (Fig. 1(b)). In the SA alloy, columnar structure was restricted to a narrow strip region, and the ratio of length over width of columnar dendritic grains was small (Fig. 2(a)). In contrast, well-developed columnar dendritic grains perpendicular to the fusion boundary were produced in the SB alloy.

Lap welded joints were made by assembling test coupons which were cut to approximately 25 mm in width and 100 mm in length parallel to the rolling direction. The details of the welding procedures and microstructural examination of the as-received alloys and welded joints have been described elsewhere [3,4]. Some of the SA sheets were further mechanically ground to reduce the thickness from 2 mm to 1.5 mm in order to eliminate the effect of varied

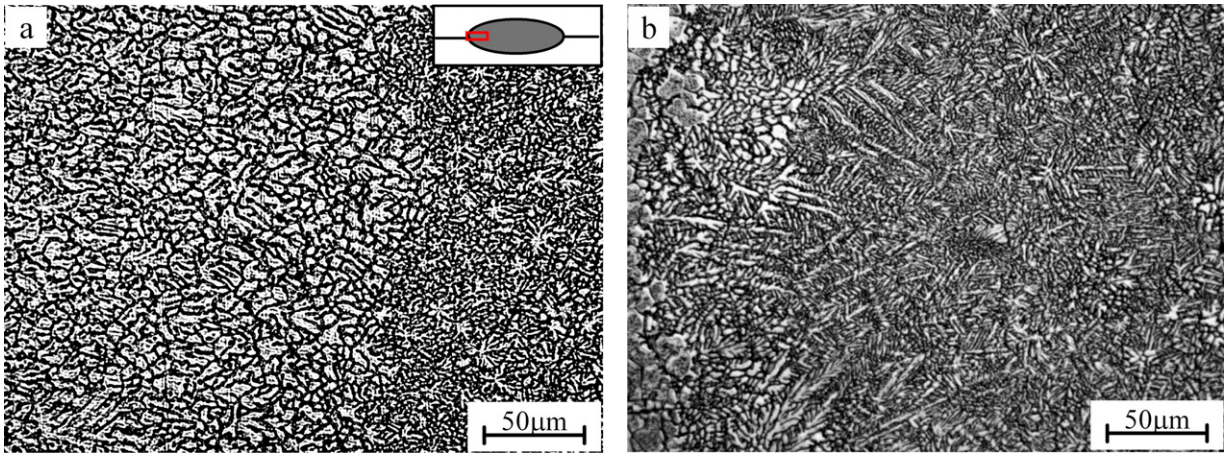

Fig. 2. Columnar dendritic structure in the vicinity of fusion boundaries of AZ31 Mg alloy resistance spot welds: (a) SA with a thickness of 2 mm and (b) SB with a thickness of 1.5 mm. The location of metallographs relative to the nuggets is indicated by a small rectangle inserted in the upper-right illustration.

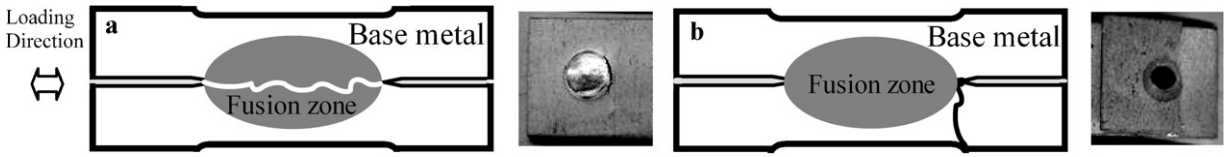

Fig. 3. Schematic illustration of fatigue failure mode: (a) interfacial failure at a higher level of cyclic load range and (b) through thickness failure at a lower level of cyclic load range.

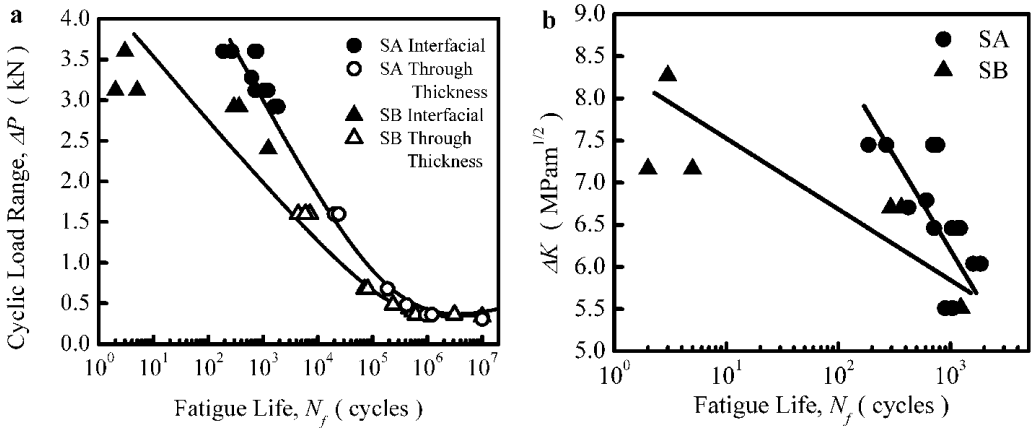

Fig. 4. Fatigue life curves of AZ31 Mg alloy welds: (a) ΔP vs. N_f and (b) ΔK vs. N_f.

thickness, and thus permitting direct comparison of weldments and their fatigue lives between the SB and SA alloys.

Load-controlled pull–pull low cycle fatigue (LCF) tests were performed on an Instron 8874 servo-hydraulic fatigue testing system at room temperature. Special care was taken to minimize the effect of misalignment between the axis of the nugget and the bonding axis. The thickness of both end sections of the welded specimens were kept to be the same as the thickness of the welded region by inserting the same thickness of sheets into grip to prevent bending moments. A triangular loading waveform was selected. Different cyclic tensile load ranges from 0.3 kN to 3.6 kN were applied at a load ratio of 0.2. The test frequency was 1 Hz, when the load range was larger than 1.6 kN. It was increased to 10 Hz so as to save time, when the load range was less than 1.6 kN. After failure, fracture surfaces were examined using a JEOL JSM-7000F scanning electron microscope (SEM). Thin foils for transmission electron microscopy (TEM) were prepared from 3-mm discs cut from the cross-sections of weld fusion zones, and then thinned by ion milling. The fatigue dislocation substructures were observed with a JEOL JEM-3010 transmission electron microscope operated at 300 kV.

3. Results

3.1. Fatigue life

Macroscopic examination revealed that failure modes of AZ31 Mg alloy welds during fatigue could be divided into interfacial failures and through thickness failures, as shown in Fig. 3. Fatigue cracks were observed to initiate and propagate parallel to the loading axis across the heat-affected and fusion zones, causing interfacial failure through nuggets, when the cyclic load range was higher than about 2.3 kN, as shown in Fig. 3(a). In contrast, fatigue cracks initiated in the heat-affected zone and propagated across circumferential base metal perpendicular to the loading axis, leading to through thickness failure, when the cyclic load range was below about 1.7 kN, as shown in Fig. 3(b).

Fig. 4(a) shows the low cycle fatigue (LCF) lives of the two types of AZ31 Mg alloy welds as a function of cyclic load range (ΔP). The LCF lives of SA welds were basically longer than those of SB at the same cyclic load range, when the cyclic load range was larger than 0.5 kN. However, the fatigue lives between SA and SB welds were similar when the cyclic load range decreased to lower than 0.5 kN. On a close examination, when the interfacial failure took place, *i.e.*, when the cyclic load range was higher than about 2.3 kN, the SA welds had a higher LCF life than SB welds, as indicated by solid circles and triangles in the upper-left side of Fig. 4(a)). However, when the through thickness failure occurred, *i.e.*, the cyclic load range was less than about 1.7 kN, the difference in fatigue lives between two AZ31 Mg alloy welds was small, as indicated by empty circles and triangles in the low-right side of Fig. 4(a).

To evaluate the effect of refined microstructure on the fatigue life of Mg alloy welds, it was necessary to eliminate the effect of the thickness of as-received sheets. Zhang [4,14,15] has successfully used cyclic stress intensity factor range (ΔK) to compare the fatigue lives of resistance spot welds joining two overlapping sheets with different thicknesses, when interfacial failure occurred. The ΔK was defined as follows:

$$\Delta K = 0.694 \frac{\Delta F_t}{d\sqrt{t}} \quad (1)$$

where ΔF_t is the load range at failure, d is the nugget diameter and t is the sheet thickness. In order to compare the fatigue lives of two groups of AZ 31 Mg alloy welds with different thichnesses, the fatigue life curves were re-plotted as a function of cyclic stress intensity factor range in the cyclic loading range larger than 2.3 kN, *i.e.*, the range of interfacial failure, or corresponding to the cyclic stress intensity factor range larger than 5.3 MPam$^{1/2}$, as shown in Fig. 4(b). SA welds still had the longer fatigue lives than SB welds. Both alloys had a similar fatigue life at the lower level of cyclic stress intensity factor ranges.

Some of the alloy SA sheets were further mechanically ground from 2 mm to the thickness of the SB alloy (1.5 mm) in order to eliminate the effect of sheet thickness. Both alloy samples were mechanically ground up to 600 mesh abrasive paper to minimize

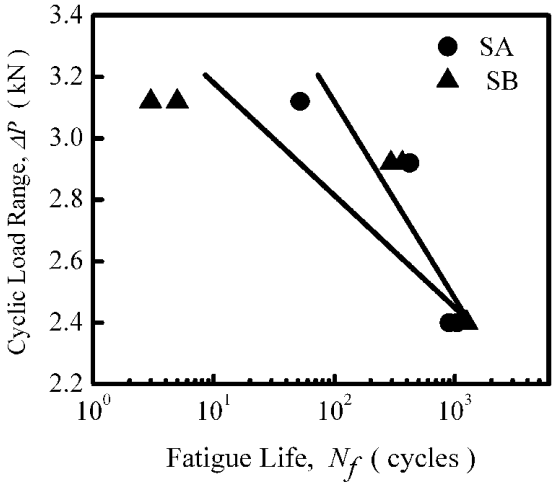

Fig. 5. A comparison of fatigue life curves between SA and SB Mg alloy welds made with an identical thickness of 1.5 mm.

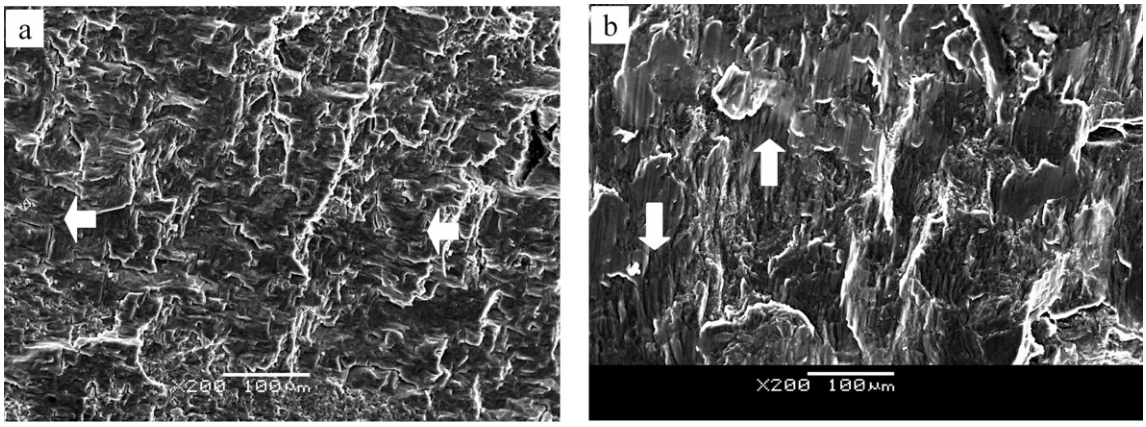

Fig. 6. A comparison of fatigue crack propagation zones in the AZ31 SA and SB welds at higher cyclic load ranges: (a) SA and (b) SB.

the effect of surface roughness of samples on welding behavior. Both SA and SB were welded using the same welding conditions. Fig. 5 illustrates a comparison of fatigue lives between SA and SB welds with the same thickness of 1.5 mm; all welds in this comparison fractured with interfacial failure due to the high cyclic loading range. Once again, SA welds exhibited longer fatigue lives than those of SB welds at the same high cyclic load range. The difference of fatigue lives dramatically decreases as the cyclic loading range decreases.

Typical fractographs of interfacial failure cases are shown in Fig. 6. Fatigue crack propagation was characterized by typical fatigue striations, which were taken as evidence of transgranular mode, as indicated by arrows in Fig. 6(a) and (b). Many plastic tear traces were observed, as shown in Fig. 6(a) and (b). Further examination showed that the spacing of fatigue striations on the SA weld fracture surfaces (Fig. 6(a)) was smaller than that of SB welds (Fig. 6(b)) tested at the same cyclic load range of 3.12 kN, corresponding to a slower crack propagation rate and longer fatigue life of SA welds in Figs. 4 and 5. The smaller fatigue striation spacing in the SA welds could be attributed to the finer dendritic structure in the fusion zone of SA welds compared to the SB welds, as shown in Fig. 1 and also explained in [3].

The fact that the SA welds had a longer fatigue life than SB when the interfacial failure occurred in the fusion zone at a higher cyclic load range implied that the fatigue resistance of fusion zones in SA welds was better than that in SB welds. Therefore, the subsequent detailed microstructure and dislocation substructure characterization has focused on the fusion zones of these welds.

3.2. Cyclic deformation substructure

The deformation substructures in the SB welds fatigue tested at different cyclic load ranges is shown in Fig. 7(a) and (b). Typical dislocation configuration comprised parallel dislocation lines, which were shown to be mostly arranged along (0 0 0 2) slip planes, when the incident electron beam was parallel to the [0 1 $\bar{1}$ 0] zone axis, as shown in Fig. 7(a). Under this observation condition, the basal planes vertically intercepts with the TEM foil surface. Therefore, straight dislocation segments lying parallel to the basal plane traces represent slip in the basal system. It is seen from Fig. 7(a) that the majority of dislocation segments were parallel to the basal slip plane trace. Further examination showed that some basal dislocation segments extended out of the basal plane trace, as indicated by arrows in Fig. 7(a). The formation of these curved dislocation lines could be attributed to the cross-slip of dislocations from the basal plane to non-basal planes, as the slipping dislocations were accumulated and blocked at obstacles on their basal planes. When the cyclic load range increased to 3.65 kN, substantial cross-slip to

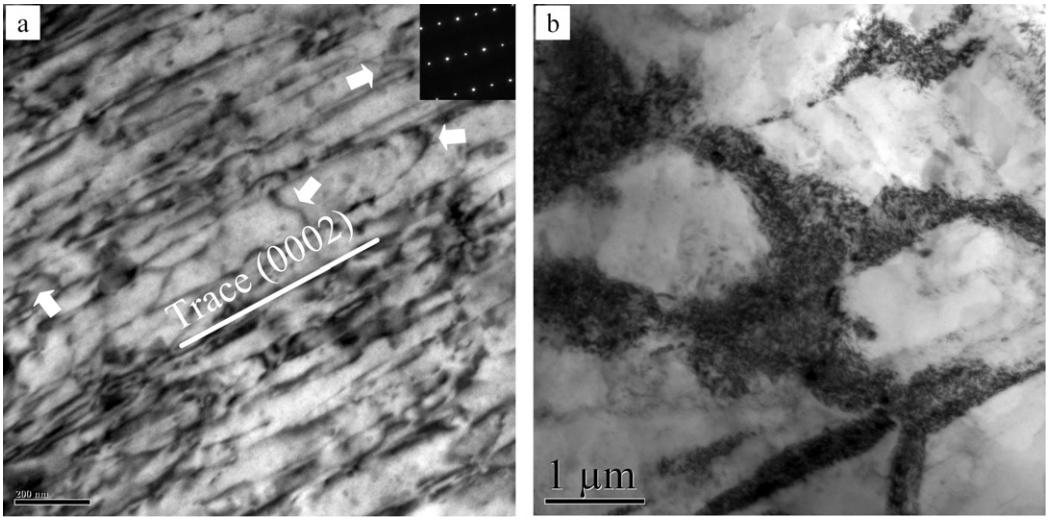

Fig. 7. Fatigue deformation structures in the SB welds at different cyclic load ranges: (a) $\Delta P = 2.92$ kN, $N_f = 125$ cycles, incident beam || [0 1 $\bar{1}$ 0] and (b) $\Delta P = 3.65$ kN, $N_f = 294$ cycles.

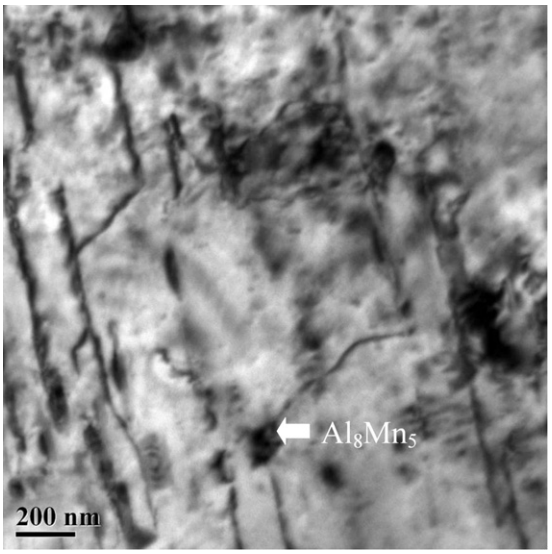

Fig. 8. Fatigue deformation structure in the SB welds.

non-basal planes occurred leading to a rapid increase of dislocation density on the non-basal planes. As a result, the fatigue dislocation configuration evolved from parallel dislocation lines to parallelogram dislocation cells, as shown in Fig. 7(b). Further examination showed that elongated dislocation lines were observed to pass the fine second-phase particles of about 0.1 μm in diameter, as indicated by an arrow in Fig. 8. In short, parallel dislocation lines were the typical dislocation pattern and planar basal slip was a predominant plastic deformation mode in the fatigued SB welds. Similar dislocation configurations and plastic deformation features have been observed in cyclically deformed hcp Mg, Ti, and Zr samples by other researchers [8,16–18].

Typical deformation substructure was composed of elongated dislocation cells in SA welds fatigue tested at different cyclic load ranges, when the incident electron beam was parallel to the $[0\,1\,\bar{1}\,1]$ zone axis, as shown in Fig. 9(a) and (b). Dense dislocation lines interacted with each other and developed into elongated dislocation cells when the cyclic load range was 2.92 kN (Fig. 9(a)). Obvious dislocation-free zones were observed around the Al_8Mn_5 particles of about 1 μm in diameter, as indicated by arrows in Fig. 9(a). This implies that the resistance to dislocation slip in the SA welds with larger Al_8Mn_5 particles was larger than that in the SB welds with finer Al_8Mn_5 particles during cyclic deformation (Fig. 8). Dislocation density increased as the cyclic load range increased to 3.65 kN; however, the cell dislocation configuration still remained, as shown in Fig. 9(b). Dense dislocation lines were visible, when the operation vector, $\boldsymbol{g}$, was equal to [0 0 0 2] (Fig. 9(b)). This implies that $\langle \boldsymbol{c}+\boldsymbol{a} \rangle$, or more precisely, $1/3\langle 1\,1\,\bar{2}\,3 \rangle$ pyramidal slip was activated in the fatigue tested SA welds, according to the $\boldsymbol{g}\cdot\boldsymbol{b}$ invisible criterion. Dislocations having a Burgers vector of $\langle \boldsymbol{a} \rangle$ were out of contrast when $\boldsymbol{g}$ was equal to [0 0 0 2]. Basal slip together with $\langle \boldsymbol{c}+\boldsymbol{a} \rangle$ pyramidal multiple slips were the primary plastic deformation features in the fatigued SA welds.

Twinning was observed to occur and acted as another plastic deformation mode in both the fatigued SB and SA welds, as shown in Fig. 10(a) and (b). This was related to the fact that the dendrite cell size in both SB and SA welds was sufficiently large (*i.e.*, ~55 μm in SA welds, and ~85 μm in the SB welds). However, it appeared that the twins were wider and longer in the SB welds (Fig. 10(a)) with coarser dendrite cells (Fig. 1(b)) compared to the SA welds (Fig. 10(b)), which had finer dendrite cells (Fig. 1(a)). These observations suggest that twinning in the fine-grained welds would be more difficult. This is also in agreement with the observations reported in [9,11–13].

4. Discussion

In a spot-welded joint, a natural notch forms at the junction of nugget between two welded sheets [14,15]. The high shear and normal stress concentration are produced at the edge of weld spot under tension-shear loading. Finite element simulation showed that the normal tensile stress concentration could reach as high as more than five times the average stress under tensile–shear loading [19]. This high normal tensile stress concentration could lead to initiate fatigue crack on the fusion boundary at the edge of weld spot, and to propagate through the nugget, when the cyclic loading range is high (Fig. 3(a)). As a result, the interfacial fracture is exhibited at high cyclic loading ranges. The strength of nugget is high enough to resist fatigue crack propagation through nuggest at the low cyclic loading ranges. Consequently, failure through thickness is displayed (Fig. 3(b)). A similar fracture mode was observed in the fatigued spot-welded DP600 steel [20].

The fatigue life of AZ31 Mg alloy welds in SB with a coarser dendrite structure was lower than that of SA with a finer dendrite

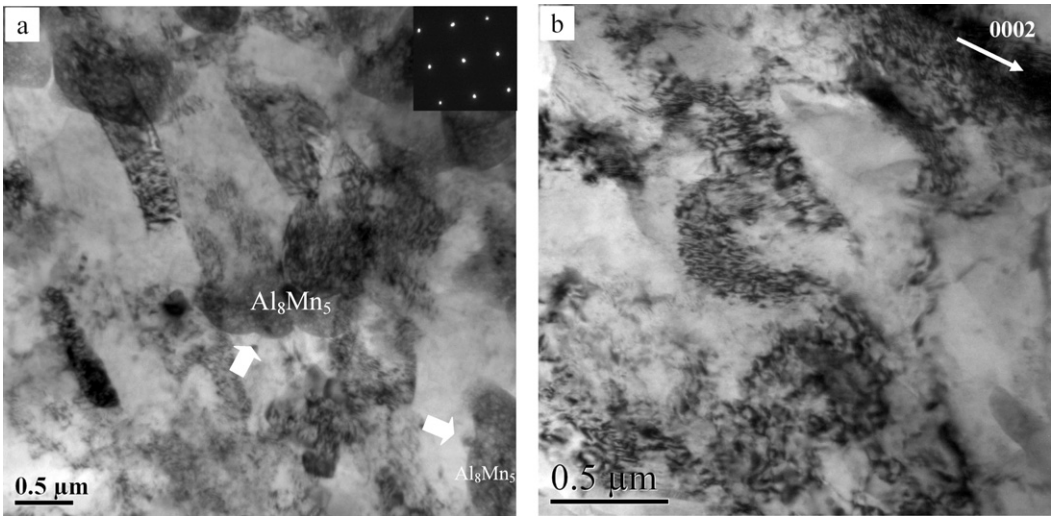

Fig. 9. Fatigue deformation structures in the SA welds at different load ranges: (a) $\Delta P = 2.92$ kN, $N_f = 1864$ cycles, incident beam || $[0\,1\,\bar{1}\,1]$ and (b) $\Delta P = 3.65$ kN, $N_f = 422$ cycles, incident beam || $[0\,1\,\bar{1}\,0]$.

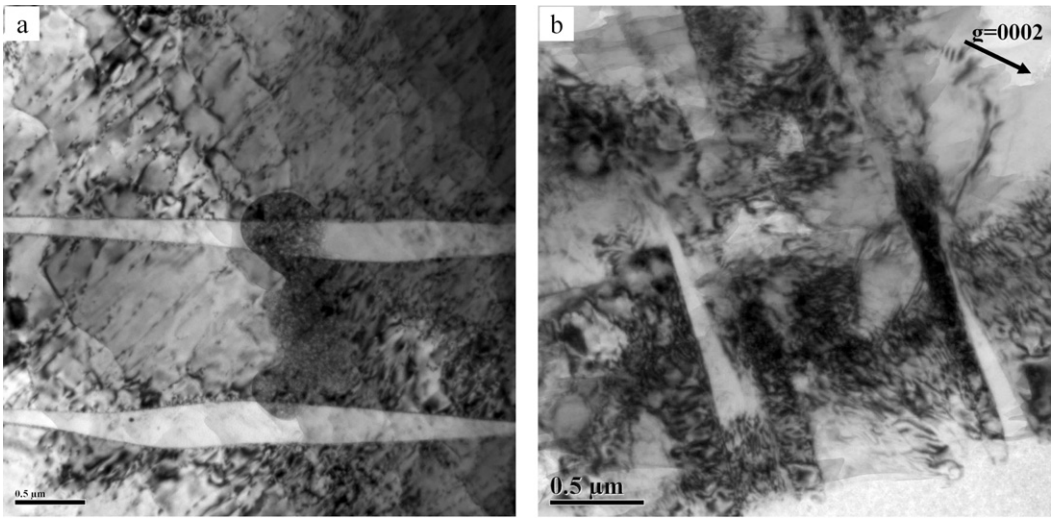

Fig. 10. Twinning in the fatigued SB and SA sample, incident beam || $[0\,1\,\bar{1}\,0]$: (a) SB and (b) SA.

structure, when interfacial failure took place across the fusion zone. The corresponding fatigue dislocation configurations changed from parallel dislocation lines and parallelogram dislocation cells in SB to elongated dislocation cells in SA. The activated slip systems changed from {0 0 0 2} single basal slip alone in the SB welds to basal slip together with pyramidal multiple slips in the SA welds. The fatigue life improvement could be rationalized in terms of the transition of plastic deformation mode in these AZ31 Mg alloy welds.

According to the reported data, the critical resolved shear stress (CRSS) of a basal slip system is approximately 1/100 those of non-basal slip systems on prismatic and pyramidal planes in single crystal Mg at room temperature [21,22]. Therefore, plastic deformation in polycrystalline Mg alloys has been thought to occur almost entirely on the (0 0 0 2) basal plane. However, the (0 0 0 2) basal slip provides only two independent slip systems, far fewer than the necessary five independent slip systems required to fulfill the von Mises criterion for homogeneous deformation of polycrystalline materials [7,23]. Consequently, plastic heterogeneity is very strong in hcp Mg alloys and may give rise to large plastic compatibility stresses between adjacent dendrite boundaries [8]. The strong slip incompatibilities in and near interdendritic regions of the Mg alloys would lead to a rapid increase of local stress concentration to a sufficiently high level to activate twinning or other possible slip systems depending on the orientation of the surrounding grains and the level of localized stress concentration.

Dislocation slip in coarse-grained SB welds was expected to be restricted to basal slip, since the welds have a well-developed columnar dendritic structure, as well as coarse equiaxed dendrites of about 85 μm diameter in which could provide a long mean free path for the mobile dislocations. Therefore, parallel dislocation lines were formed in the fatigued SB welds (Fig. 7(a)). As the applied cyclic load range increased, the slipping dislocations piled up and accumulated at obstacles on the basal planes, local stress concentrations would be produced to activate cross-slip to non-basal planes. As a result, cross-slipping of ***a*** dislocation to non-basal planes was significantly activated resulting in the formation of parallelogram dislocation cells at high cyclic load ranges (Fig. 7(b)).

Localized stress concentration is proportional to the grain size at a given applied stress [23]. It is much higher in coarse-grained samples than that in fine-grained samples, since the former would have a longer mean free path of the mobile dislocations than the latter, leading to pile-up of more dislocations against obstacles as sessile dislocations. This would result in a magnified internal stress at the head of the pile-up which would cause sources in certain secondary systems to operate [23]. On the other hand, deformation twinning becomes more active in coarse grains during plastic deformation, because the critical shear stress for twinning in fine-grained specimens was calculated to be higher than that in coarse-grained ones [24]. Therefore, the localized stress concentrations in coarse grains could easily reach the critical shear stress for twinning at a given applied stress. Consequently, deformation twinning was more easily activated in the coarse-grained SB welds due to sufficient stress concentration and the lower critical shear stress of twinning. In comparison, the level of local stress concentration would decrease and the critical shear stress for twinning increase, leading to less extensive twinning in the SA welds with refined grains. However, the number of grains oriented for favorable non-basal slip is expected to increase in the fine-grained SA welds. Under such a circumstance the pyramidal multiple slips and twinning could be simultaneously activated in the SA welds. Similar results have been reported in [8,11]. The activation of basal and pyramidal slips together with twinning can provide five independent slip systems to satisfy the von Mises criterion for sustained plastic deformation of polycrystals [7]. As a result, dislocation cells became a predominant dislocation configuration in the fatigue tested fine-grained SA welds (Fig. 9).

In our previous study [3], three scales of particles were observed in these two AZ31 Mg alloys in the as-received and welded conditions. Micron-sized Al_8Mn_5 particles (4–10 μm in diameter) were only observed in the SA welds. Submicron-sized Al_8Mn_5 second-phase particles (0.09–0.4 μm in diameter) and nano-$Mg_{17}(Al, Zn)_{12}$ precipitates (0.1 μm in diameter) were detected in both SA and SB welds. The intermetallic compounds are harder than the matrix of Mg. The presence of harder second-phase particles in the fusion zone played an important role of dispersion strengthening by the Orowan dislocation bypass strengthening mechanism in the SA welds with the large-size of particles [18]. The interaction between dislocations and second-phase particles leads to an increase of the resistance to dislocation slip [23]. A transition from planar single slip to multiple slips could be induced, and the fatigue lifetime of the alloy could be enhanced. However, further work is needed to understand in detail the effect of second-phase particles on plastic deformation behavior and their relative contributions to fatigue life improvement of Mg alloy welds.

Better fatigue properties have generally been related to a higher degree of dispersion of slip systems for hcp metals [7,23,25]. Therefore, longer fatigue life can be expected in the SA welds than that in the SB welds due to the increase in the number and dispersibility of slip systems in the fusion zone during cyclic deformation under conditions where interfacial fracture occurs at a higher level of cyclic load range (*i.e.*, in the LCF range of about $N_f < 3 \times 10^3$ cycles), as shown in Fig. 4.

The currently observed effect of the size of microstructural features on fatigue life can also be corroborated from a perspective of fatigue crack growth resistance in cast Mg alloys as reported in [26]. *In situ* observations of low-cycle fatigue damage by Gall et al. [26] showed that fatigue cracks nucleated and grew along persistent slip bands (PSBs) in the cast AM60B Mg alloy. The strong slip incompatibilities between adjacent dendrite cells created high mismatch stresses in and near interdendritic regions and facilitated rapid PSB and crack formation. PSB formation and subsequent cracking were often favored in larger dendrite cells because of the relatively larger dislocation pile-up length and, thus, higher local stresses. Cracks that formed at PSBs nearly instantaneously spanned the entire length of the slip band, rather than slowly propagating along the slip band. Consequently, the cast AM60 Mg alloy with the finer dendrite size displayed the higher resistance to fatigue crack growth and an improved fatigue life [26]. AM30 Mg alloy with smaller grains was also observed to exhibit a greater fatigue resistance compared to specimens with larger grains [27]. Therefore, the SA welds containing finer dendrite cells could be expected to have a stronger resistance to fatigue crack propagation and a longer fatigue life than the SB welds with coarser dendrite cells.

5. Conclusions and summary

1. AZ31 SA resistance spot welds with a refined fusion zone microstructure had a longer fatigue life than that of AZ31 SB welds with a coarse fusion zone microstructure, when interfacial failure across fusion zone occurred at a higher level of cyclic load range larger than 2.3 kN.
2. Typical dislocation configurations in the fusion zone of the SA welds consisted of elongated dislocation cells. In comparison, elongated parallel dislocation lines and parallelogram dislocation cells were observed in the SB welds.
3. Deformation mode in the AZ31 welds evolved from $\{0\,0\,0\,2\}$ single basal slip in the SB alloy welds to $1/3\langle 1\,1\,\bar{2}\,3\rangle$ pyramidal combined with $\{0\,0\,0\,2\}$ basal slips in the SA alloy welds.
4. Twinning was observed to serve as another important deformation mode in both SA and SB welds. However, more twins appeared to be present in the coarser-grained SB welds. This may be due to the strong slip incompatibilities causing a rapid increase of local stress concentration to a sufficiently high level to activate twinning in neighboring dendrite cells which had the higher stress concentration and the lower critical shear stress for twinning.
5. Pyramidal multiple slips and twinning were simultaneously activated in the finer-grained SA welds probably due to the lower stress concentrations and the high critical shear stress for twinning. This led to an increase of the amount and dispersibility of slip systems in the SA welds, thus a longer fatigue life than that of the SB welds.

Acknowledgments

This research is financially supported by the Natural Sciences and Engineering Research Council (NSERC) of Canada in the Framework of Strategic Magnesium Network Program (MagNet) and AUTO21 Network Centers of Excellence of Canada. LX would like to thank NSERC for the Postgraduate Scholarship. We acknowledge partial support of this research by POSCO. The authors would also like to thank S.B. Behravesh for help with part of the fatigue testing.

References

[1] L.M. Liu, Z.D. Zhang, G. Song, L. Wang, Metall. Mater. Trans. A 38 (2007) 649–658.
[2] L. Commin, M. Dumont, J.E. Masse, L. Barrallier, Acta Mater. 57 (2009) 326–334.
[3] L. Xiao, R. Liu, Y. Zhou, S. Esmaeili, Metall. Mater. Trans. A 41 (2010) 1511–1522.
[4] L. Liu, L. Xiao, J.C. Feng, Y.H. Tian, S.Q. Zhou, Y. Zhou, Metall. Mater. Trans. A 41 (2010) 2642–2650.
[5] S. Kou, Welding Metallurgy, 2nd edition, Wiley Interscience/John Wiley & Sons Inc., Hoboken, NJ, 2003.
[6] S.A. David, J.M. Vitek, Int. Mater. Rev. 34 (1989) 213–245.
[7] M.H. Yoo, Metall. Mater. Trans. A 12 (1981) 409–418.
[8] J. Koike, T. Kobayashi, T. Mukai, H. Watanabe, M. Suzuki, K. Murayama, K. Higashi, Acta Mater. 51 (2003) 2055–2065.
[9] C.H. Caceres, T. Sumitomo, M. Veidt, Acta Mater. 51 (2003) 6211–6218.
[10] M.R. Barnett, Z. Keshavarz, M.D. Nave, Metall. Mater. Trans. A 35 (2005) 1697–1704.
[11] H.A. Patel, D.L. Chen, S.D. Bhole, K. Sadayappan, Mater. Sci. Eng. A 528 (2010) 208–219.
[12] M.A. Meyers, O. Voringer, V.A. Lubarda, Acta Mater. 49 (2002) 4025.
[13] H. Conrad, J.J. Narayan, Acta Mater. 50 (2002) 5067–5078.
[14] S. Zhang, Int. J. Fract. 88 (1997) 167–185.
[15] S. Zhang, Weld. J. 80 (2001) 201s–203s.
[16] C.Q. Chen, Y.T. Pei, J.T.M. De Hosson, Acta Mater. 58 (2010) 189–200.
[17] L. Xiao, Y. Umakoshi, Philos. Mag. 83 (2003) 3407–3426.
[18] L. Xiao, H. Gu, Metall. Mater. Trans. A 28 (1997) 1021–1033.
[19] B. Chang, Y. Shi, L. Lu, J. Mater. Process. Technol. 108 (2001) 307–313.
[20] C. Ma, D.L. Chen, S.D. Bhole, G. Boudreau, A. Lee, E. Biro, Mater. Sci. Eng. A 485 (2008) 334–346.
[21] T. Obara, H. Yoshinaga, S. Morozumi, Acta Metall. 21 (1973) 845–853.
[22] F.F. Stohr, J.P. Poirier, Philos. Mag. 25 (1972) 1313–1329.
[23] R.W.K. Honeycombe, The Plastic Deformation of Metals, 2nd edition, Edward Arnold Publishers Ltd., London, 1984.
[24] H. Wang, Y.L. Xu, Q.Y. Sun, L. Xiao, J. Sun, P. Ge, Metall. Mater. Trans. A 40 (2009) 2631–2643.
[25] S. Suresh, Fatigue of Materials, Cambridge University Press, Cambridge/New York, 1998.
[26] K. Gall, G. Biallas, H.J. Maier, P. Gullett, M.F. Horstemeyer, D.L. Mcdowell, Metall. Mater. Trans. A 35 (2004) 321–331.
[27] J.D. Bernard, J.B. Jordon, M.F. Horstemeyer, H. El Kadiri, J. Baird, D. Lamb, A.A. Luo, Scr. Mater. 63 (2010) 751–756.